

Biochar production through slow pyrolysis of different biomass materials: Seeking the best operating conditions

Joan J. Manyà^{a,b,*}, Manuel Azuara^{b,c}, José A. Manso^b

^a *Aragón Institute of Engineering Research (I3A)*, ^b *Technological College of Huesca*, and ^c *Institute of Nanoscience of Aragón (INA), University of Zaragoza, crta. Cuarte s/n, Huesca E-22071, Spain*

* Corresponding author. Aragón Institute of Engineering Research (I3A), Technological College of Huesca, University of Zaragoza, crta. Cuarte s/n, Huesca E-22071, Spain.

E-mail: joanjoma@unizar.es (Joan J. Manyà).

Keywords

Biochar; Residual biomass; Pressurized slow pyrolysis; Carbon sequestration potential; Produced gas

ABSTRACT

The effect of three operating parameters (peak temperature, pressure, and pyrolysis atmosphere) during the slow pyrolysis of three biomass sources (corn stover, vine shoots, and two-phase olive mill waste) was extensively analyzed. A 2-level full factorial design of experiments was adopted to assess the effect of the above-mentioned factors on the potential stability of biochar as well as the yields of the main pyrolysis products. To evaluate the effect of the biomass feedstock, the design was divided into three blocks (one per biomass feedstock). Results from the statistical analyses indicated that the properties of biochar related to its potential stability were mainly affected by the peak temperature and, to a lesser extent, the biomass feedstock. A significant increase in the yield of produced gas was observed when pressure was raised. This increase in the total gas yield was in part due to a higher release of CO, CH₄, and H₂. Using a pyrolysis atmosphere of CO₂ (instead of N₂) did not result in any remarkable change in neither the distribution of the pyrolysis products nor the potential stability of biochar. However, when CO₂ was used as carrier gas, a significant increase in the yield of CO, at the expense of produced CO₂, was observed. The findings reported herein suggest that processing biomass through pressurized slow pyrolysis under CO₂ atmosphere is interesting to simultaneously obtain two valuable products: a biochar with an appropriate carbon sequestration potential, and a produced gas with an appropriate composition for energy recovery purposes.

1. Introduction

Concerns about climate change and improvement of soil quality in a sustainable manner have generated much interest in biochar, a form of charred organic matter derived from biomass, which when applied to soil in a deliberate manner has the potential to improve carbon sequestration as well as soil productivity [1]. Biochar could enhance the capacity of soils for holding water and nutrients and, thus, reducing the use of chemical fertilizers. Nevertheless, the effects of biochar and the requirements on its properties for soil amendment and carbon sequestration purposes have not fully been established [2]. The influence of numerous parameters (such as biochar production process and operating conditions, soil properties, and biomass feedstock) on the carbon sequestration potential as well as soil-biochar interactions is still not well understood.

The economic feasibility of biochar systems for agronomic benefits depends on numerous factors including the biomass feedstock selection and transportation requirements. There is increasing uncertainty about the potential of such systems for commercial exploitation. Thus, developing more efficient production processes and novel alternative or added-value uses for biochar can lead to a more competitive technology.

Pyrolysis is a thermochemical decomposition process during which biomass is heated at moderate temperature (typically 350–650 °C) in the absence of oxygen. The process results in the formation of three main products: charcoal (i.e., biochar), a volatile matter which can further be condensed to liquid phase (bio-oil), and the remaining so-called “non-condensable” gases, like CO, CO₂, CH₄, and H₂. Depending upon the residence time, peak temperature, and heating rate the pyrolysis process is sub-divided into three categories: slow, intermediate and fast pyrolysis. Slow pyrolysis is usually preferred to produce biochar, with gas as co-product. It is a relatively simple

and robust process which can be applicable to small-scale and farm-based production of biochar [3,4].

In spite of the relatively simplicity of the slow pyrolysis process, the yields and properties of products (including those of biochar) can be largely affected by the operating conditions (e.g., peak temperature, residence time of the vapor phase, pressure, and particle size). In addition, the nature of the biomass source also plays a key role in determining the yield and properties of produced biochar.

An interesting option to improve the carbonization efficiency (i.e., fixed-carbon yield [5]) is to increase pressure. In this sense, most of the previous studies on pressurized pyrolysis reported on an increase in both the biochar and gas yields, at the expense of the organic condensable fraction [6–8]. In these studies, however, the effect of a moderate pressure (0.5–5.0 MPa) was measured without keeping constant the residence time of the inert gas within the reactor. In order to investigate the true effect of pressure, some researchers conducted pressurized pyrolysis experiments at constant gas residence time [4,9–12]. Results from these alternative studies indicated that the effect of pressure on the biochar yield is still unclear, since negligible [11,12], positive [9] and even negative [4,10] correlations were found.

Another interesting option to improve the efficiency of the slow pyrolysis process, especially in terms of economics saving, is replacing the use of a relatively expensive inert gas (e.g., N₂) with CO₂ coming from residual flue gases [13]. In other words, the flue gas generated after combustion of pyrolysis gas can be used as pyrolysis gas environment. Nevertheless, research is required to understand the effects of modifying the pyrolysis environment (i.e., from pure N₂ to a flue gas containing CO₂) on the distribution of the pyrolysis products as well as on the properties of produced biochar (e.g., the properties related to its carbon sequestration potential). In this sense, results from

a preliminary study [14] indicated that the use of CO₂ instead of N₂ did not significantly affect the properties of biochar related to its carbon sequestration potential (e.g., fixed-carbon content and molar H:C and O:C ratios).

In addition to the fixed carbon content and molar H:C and O:C ratios, several approaches have been proposed to estimate the long-term stability of biochar. Among them, two relatively easy techniques have recently gained attention: (1) the recalcitrance index (R_{50}), which was proposed by Harvey et al. [15] and is based on the relative thermal stability of a given biochar to that of graphite; and (2) a method developed at the UK Biochar Research Center, which is based on the oxidation of biochars using H₂O₂ to accelerate the “aging” and, hence, the oxidative loss of carbon [16,17].

The specific aim of this study is to determine the effect of certain operating conditions (peak temperature, pressure at constant gas residence time, and pyrolysis environment) on several properties of biochar produced through slow pyrolysis of three different sources: corn stover, vine shoots, and two-phase olive mill waste. Special attention is focused on how the operating conditions can affect the properties of biochar related to its potential stability (i.e., carbon sequestration potential). In addition, the yield and composition of the pyrolysis gas was also determined as a function of the tested operating conditions.

2. Experimental section

2.1. Materials

Three waste biomass materials, all of them generated in the province of Huesca (Spain), were used in the present study: (i) corn stover (CS) containing corncob (15.5 wt.%), leaf (4.3 wt.%) and stalk (80.2 wt.%); (ii) two-phase olive mill waste (TPOMW), which was sun-dried in the field for several months at the premises of an extra-virgin olive oil factory; and (iii) vine shoots (VS) supplied by a local winery.

Proximate analyses were performed in quadruplicate according to ASTM standards (D3173 for moisture, D3174 for ash, and D3175 for volatile matter), whereas elemental analyses were carried out using a CHNS analyzer from Leco Corporation (USA). In addition, the ash composition expressed as weight percentages of the equivalent oxides was measured using an ADVANT'XP+ XRF spectrometer from Thermo ARL (Switzerland).

2.2. Experimental devices and procedures

The fixed-bed pyrolysis reactor consisted of a cylindrical and vertical reactor (140 mm inside diameter and 465 mm long) made of Sandvik 253 MA stainless steel (EN 1.4835; X9CrNiSiNc21-11-2). The reactor was heated by two electric resistances of 2.1 kW. A basket of 4 L, made of Monel 400 alloy (Ni65Cu33Fe2) wire mesh, was used to put the biomass into the reactor. The temperature inside the bed was measured using four thermocouples placed in a thermowell at different heights. More details regarding the configuration of the reactor are available elsewhere [4,12,14]. The pressure of the system was controlled through a back-pressure regulator. A schematic diagram of the experimental setup is given in Fig. 1.

The mass flow rate at STP conditions of the carrier gas (N_2 or CO_2) was adjusted as a function of the absolute pressure (0.1–1.0 MPa) to keep the real flow rate of the carrier gas within the reactor (at the highest temperature) at a constant value of 1.85 L min^{-1} . After each experiment, the condensed fraction was recovered directly from the condensers without using any solvent as wash liquid. The glass traps were weighted before and after each experimental run to determine the total mass of liquid. The content of water in the condensable fraction was measured using a Karl-Fischer volumetric titrator from Metrohm (Switzerland). The composition of the gas fraction (N_2 , CO_2 , CO , CH_4 , C_2H_x and H_2) was determined using an Agilent micro-GC equipped with two analytical

columns: a PoraPlot Q (using He as carrier gas) and a Molsieve 5A (using Ar as carrier gas). The mass of produced gas was calculated from the N₂ mass balances.

The initial sample mass of biomass, which depends on the bulk density of the feedstock, was approximately of 250, 400, and 750 g for CS, VS, and TPOMW; respectively. Particle size distributions were determined by sieving according to ISO 3310-1 standard. Fig. 2 displays the differential and cumulative distributions for each biomass feedstock. The median (d_{50}) and surface-volume mean (calculated as the harmonic mean of the cumulative mass fraction [18]) diameters for each biomass feedstock are also given in Fig. 2. In the case of CS and VS, we used large particles with the aim of avoiding the high energy-consuming milling pre-treatments. Furthermore, using large biomass particles can lead to an improvement in carbonization efficiency (i.e., biochars with higher fixed-carbon contents) as a consequence of an enhancement of the secondary charring reactions at intra-particle level [19].

The void-volume fractions in the pyrolysis reactor were estimated to be in the range of 0.85–0.90. These estimates were calculated using the experimentally measured bulk densities (268, 111, and 70 kg m⁻³ for TPOMW, VS, and CS; respectively) and the particle densities available in the literature (1394, 1250, and 1170 kg m⁻³ for TPOMW [20], VS [21], and CS [22]; respectively). Given that the void-volume fraction was almost constant regardless of the biomass feedstock, an almost constant gas-hourly space velocity (GHSV) of 17.2 h⁻¹ can be assumed for all the experiments.

Pyrolysis experiments were conducted according to a 2-level full factorial design with three factors: peak temperature (400–600 °C), absolute pressure (0.1–1.0 MPa), and carrier gas (measured as the mole fraction of CO₂ in a mixture N₂/CO₂, and ranging from 0 to 0.95). Three replicates at the center point (500 °C, 0.55 MPa, and a CO₂ mole fraction of 0.48) were conducted for each

biomass feedstock to simultaneously estimate the experimental error and the overall curvature effect [23]. Three blocks (one per each feedstock) were added to the design in order to analyze the effect of the biomass source on the average values. All the statistical calculations were conducted using R software (version 3.3.3). The matrix of the design of experiments is shown in Table S1 (Supplementary Data).

In order to get an estimate of the concentration of the main biomass constituents, additional pyrolysis tests were conducted in an atmospheric thermobalance (a MK2 microbalance with a readability of 0.1 μg from CI Precision, UK). Initial sample masses of 25 mg were heated at a linear heating rate of 5 $^{\circ}\text{C min}^{-1}$ (highest temperature = 600 $^{\circ}\text{C}$) under an atmosphere of N_2 at a flow rate of 200 mL (STP) min^{-1} .

2.3. Characterization of the pyrolysis products

The mass yields of biochar, water, condensable organics and produced gas (y_{char} , y_{water} , y_{org} and y_{gas} , respectively) were calculated in a dry-ash-free (daf) basis. Biochar samples were characterized by proximate and elemental analyses according to the same procedures described in Section 2.1. The mass fraction of fixed carbon in the biochar (x_{FC}) was calculated from the proximate analysis data, whereas the molar H:C and O:C ratios were calculated from the elemental analysis data.

Temperature-programmed oxidation (TPO) of the biochars was conducted using the same thermobalance described above. Approximately 10 mg of sample was heated in N_2 -diluted air (100 mL STP min^{-1}) from room temperature to 950 $^{\circ}\text{C}$ at a linear heating rate of 10 $^{\circ}\text{C min}^{-1}$. The R_{50} index was then calculated from the TPO data using the following equation:

$$R_{50,x} = T_{50,x} / T_{50,g} \quad (1)$$

where $T_{50,x}$ and $T_{50,g}$ are the temperatures corresponding to 50% of mass loss of biochar and graphite, respectively.

Direct oxidation of biochars was performed according to the procedure described by Cross and Sohi (Edinburgh stability tool) [17]. Briefly: biochar samples containing 0.1 g of C were milled to a fine powder in a ball mill and then treated in a test tube with 7 mL of an aqueous solution of 5% H₂O₂, initially at room temperature and then at 80 °C for 48 h. The samples were then dried in an oven at 105 °C overnight. The “*stable C*” was expressed as the percentage of the initial 0.1 g of C that remains after oxidation.

3. Results and discussion

Results from proximate, elemental and ash analyses are summarized in Table 1. The experimental results obtained from the factorial design of experiments are given in Supplementary Data (Tables S2 and S3). The mass-balance closures for all the pyrolysis tests (above 95%) are given in Table S2. The mass yields of the different pyrolysis products (y_{char} , y_{water} , y_{org} and y_{gas}) were then calculated attributing the error in the mass-balance closure to minor inaccuracies in determining the mass of produced gas.

3.1. Effects on the yield of biochar and its potential stability

For the response variables which are related to the biochar yield as well as carbon sequestration potential (i.e., y_{char} , x_{FC} , molar H:C and O:C ratios, R_{50} index, and “*stable C*”), Table S2 shows the data obtained for each experimental run (a total of 11 per block).

The structure of the regression model, which was used as an approximation for statistical testing, was the following:

$$\hat{y} = \beta_0 + \beta_1 T + \beta_2 P + \beta_3 CO_2 + \beta_{12} T \cdot P + \beta_{13} T \cdot CO_2 + \beta_{23} P \cdot CO_2 + \beta_{123} P \cdot T \cdot CO_2 \quad (2)$$

where β_0 , β_i , β_{ij} , and β_{ijk} are the intercept, linear, 2-way interaction, and 3-way interaction coefficients; respectively.

Table 2 lists, for each response variable, the estimated regression coefficients for coded factors (-1, +1) and associated p -values (from t -tests), as well as the adjusted R^2 values. In the event that the regression coefficient for the overall curvature term becomes significant, a second-order regression model (including pure quadratic terms for each factor) is needed in order to improve the accuracy of model predictions. In addition, the regression coefficients estimated for the blocks are also presented in Table 2. The regression coefficient for a given block represents the difference between the mean of the response for this block and the overall mean of the response.

To get a graphical interpretation of the results, the normal plots of standardized effects (for a significance level of 0.05) for the above-mentioned response variables are shown in Fig. 3. From these plots, and also from the statistical data listed in Table 2, it can be concluded that the peak temperature was the most influential factor on the potential stability of biochar, since its effect was statistically significant for all the response variables analyzed in this section. As expected, an increase in the peak temperature led to an increase in x_{FC} , R_{50} index and “*stable C*” as well as a decrease in both the H:C and O:C molar ratios. The direction of these significant effects is consistent with the idea that any of these variables related to the potential stability of biochar can be taken as a rough indicator of the carbon sequestration potential.

It should be emphasized that the significant effects of the peak temperature were found from the experimental data obtained using three different biomass sources (CS, VS, and TPOMW). In other words, increasing the peak temperature from 400 to 600 °C led to biochars with higher carbon sequestration potential, regardless of the biomass processed in the present study. This finding is not contradictory to the fact that the regression coefficients for the block terms were significant in several cases (see Table 2). This means that, as expected, the potential stability of biochar is dependent on the type of biomass feedstock. As an example, the percentages of “*stable C*” and

fixed-carbon contents (x_{FC}) obtained for corn stover-derived biochars were, on average, significantly higher than those obtained for the other two biomass sources.

From the statistics shown in Table 2 and Fig. 3, it can also be deduced that an increase in the absolute pressure led to a significant increase in x_{FC} and a significant decrease in the molar H:C ratio. However, the improvement of these indicators of the potential stability of biochar was quantitatively much lower than that observed for an increase in the peak temperature. In regard to the effect of the pyrolysis atmosphere, a slightly significant decrease in the molar H:C ratio was observed when the carrier gas was mainly composed of CO_2 .

It is also interesting to highlight that the curvature term was significant for all response variables with the exception of the R_{50} index. This finding means that an augmentation to a central composite design should be considered in further studies in order to define more accurately the location of the optimal conditions (via Response Surface Methodology) [23]. In regard with this, it can be possible that the optimal value for a given factor (e.g., the peak temperature that minimizes the molar H:C ratio) could be lower than the highest level (e.g., below 600 °C for the peak temperature factor and/or below 1.0 MPa for the absolute pressure factor).

Regarding the biochar yield (y_{char}), the peak temperature was also the most influential factor. As expected and in agreement with a number of previous studies [6,7,24–28], a decrease in the production of biochar was associated to an increase in the peak temperature. The biochar yield was also significantly affected by an increase in the absolute pressure, resulting in a slightly decrease in y_{char} . This finding, which was already observed in previous studies [4,10], can be explained by two main reasons. First, pressurized pyrolysis can cause an enhancement of the steam gasification reaction kinetics leading to non-negligible reaction rates, even at relatively low temperatures. Second, an increase in the mass flow rate of carrier gas for pressurized pyrolysis can lead to a

reduction of the concentration of volatiles within the reactor (i.e., dilution effect), possibly resulting in a lower extent of the secondary charring reactions. No significant effect of the composition of the carrier gas on the yield of biochar was found.

As can be seen from the regression coefficients for the block terms listed in Table 2, the biochar yield was also dependent on the type of biomass feedstock. Higher mass yields of biochar than average were obtained when TPOMW was pyrolyzed. This fact could be explained by differences in the concentration of the biomass constituents (hemicelluloses, cellulose and lignin). Thermogravimetric measurements under dynamic heating conditions were conducted for the three biomass sources in order to estimate the contents of the biomass constituents. The experimental differential thermogravimetric (DTG) curves were deconvoluted into three peaks using the “Peak Analyzer” tool implemented in OriginPro version 9.0 (OriginLab, USA). These three peaks are associated to the devolatilization of hemicelluloses (peak 1), cellulose (peak 2), and lignin (peak 3). Fig. 4 shows the deconvoluted DTG curves obtained for the three biomass sources (CS, VS, and TPOMW). From Fig. 4, it can be deduced that the apparent lignin content (which is associated to peak 3) for TPOMW is considerably higher than that determined for CS and VS. This is consistent with the fact that lignin is the biomass constituent which leads to the highest char yield [29]. In summary, the composition of the biomass source in terms of its main lignocellulosic biomass constituents appears to be a key parameter in explaining the differences observed in the biochar yield.

Regarding the possible effects of alkali and alkaline earth metal species AAEMs, the differences in the content of Ca and K between the three biomass sources (deduced from Table 1) were probably too low to observe any quantitative effect on the biochar yield. Nevertheless, as evidenced in Fig. 4, the temperature corresponding to the highest devolatilization rate (for the thermogravimetric

pyrolysis tests) was dependent on the biomass feedstock (303 °C for TPOMW, 330 °C for CS, and 353 °C for VS). This fact could be related to the role of the AAEMs, which can promote the biomass decomposition at lower temperatures. In this sense, it should be noted that the temperature for the highest devolatilization rate decreased as the content of Ca plus K in the biomass feedstock increased (1.17, 0.752, and 0.563 g for each 100 g of raw biomass for TPOMW, CS, and VS; respectively).

3.2. Effects on the yield of pyrolysis gas and its composition

From analyzing the statistical results listed in Table 3 (regression models) and shown in Fig. 5 (normal plots of standardized effects), it can be concluded that the absolute pressure plays a key role in determining the yield of the produced pyrolysis gas as well as the yield of the individual gaseous species analyzed in the present study.

The yield of total gas (y_{gas}) significantly increased when the peak temperature was increased from 400 to 600 °C (at the expense of the yield of biochar) or the absolute pressure was raised from 0.1 to 1.0 MPa (at the expense of the yield of produced water). The positive effect of the peak temperature on the gas yield was certainly expected because of the higher extent of devolatilization processes. In addition, an increased temperature can result in a promotion of the secondary cracking reactions, given the relatively high residence time of the pyrolysis vapors within the reactor.

Concerning the favorable effect of the absolute pressure on the produced gas at the expense of the yield of water (y_{water}), an interpretation can be envisaged to explain this finding. The vapor pressure of volatiles increases with raising the absolute pressure, leading to an acceleration of the cross-linking reactions and the subsequent higher production of char and gas at relatively low process temperatures [30]. Nevertheless, above a certain temperature, the extent of the steam-char gasification reaction could be non-negligible at high pressure [31], especially when the content of

AAEMs in the biomass feedstock is non-negligible. In other words, the formation of char could be enhanced with the increasing pressure, mainly due to the restricted transport of volatiles. However, some carbon can simultaneously react with steam, resulting in a decrease in the overall yields of biochar and water and a parallel increase in the overall yield of pyrolysis gas.

With regard to the effect of the biomass source on the yields of produced water and gas, Table 3 shows statistically significant regression coefficients for both blocks 2 (associated to VS) and 3 (associated to TPOMW). This fact could also be explained by differences in the content and activity of K plus Ca between the biomass sources. Given that the AAEMs contained in the TPOMW feedstock seems to be highly active compared with the other biomass samples (see Fig. 4), a higher yield of gas (and a lower yield of water) than average was expected. The same argumentation is valid to explain the lower-than-average gas yields (and higher-than-average yields of water) observed for the VS feedstock, which seems to contain the least active AAEMs.

No statistically significant effects (neither for y_{gas} nor for y_{water}) were found for the pyrolysis atmosphere. This finding is apparently in disagreement with earlier observations from Pilon and Lavoie [13] (for pyrolysis of switchgrass at 500 °C) and Azuara et al. [14] (for pyrolysis of vine shoots at 600 °C). In these two studies, a slightly significant increase in the yield of gas under an atmosphere of CO₂ was reported for experiments conducted at atmospheric pressure. However, and as revealed from the statistical data reported in Table 3, the effect of using an atmosphere of CO₂ on the yield of gas was not significant when the experimental data obtained from the pyrolysis of three different biomass sources were simultaneously analyzed.

Concerning the yield of condensable organic compounds (y_{org}), there were no statistically significant effects of any factor (see Table 3). The lack of statistical influence of the peak temperature could be explained by a higher extent of the thermal cracking reactions when this factor

was raised. This could balance the higher release of volatiles caused by a higher devolatilization of the biomass constituents at high peak temperatures.

From the results shown in Table 3 and Fig. 5, it can also be concluded that the cumulative yield of all the gaseous species analyzed was significantly affected by the peak temperature and the absolute pressure. As has been mentioned above to explain the dependence of y_{gas} , the observed increases in the yields of the gaseous species can be attributed to the higher decomposition of the biomass constituents, especially lignin, which decomposes over a very wide temperature range (see Fig. 4). In addition, the enhancement of the thermal cracking of the primary volatiles at high temperatures (leading to an additional formation of permanent gaseous compounds) can also explain the observed effect of the peak temperature.

The increase in the yield of CO_2 with the increased pressure could be explained by a promotion of decarboxylation routes for both hemicelluloses and cellulose, as suggested by Qian et al. [9] in an earlier study on pressurized pyrolysis of rice husks. Moreover, additional reasons for the effect of the absolute pressure on the yields of gaseous species can be gleaned from analyzing the data reported in Table 4. In this sense, an increase in the absolute pressure from 0.1 to 1.0 MPa can favor the production of CO_2 through reactions #2 (Boudouard) and #6 (reverse dry reforming). In addition, the observed increase in the yield of CH_4 with the increased pressure can be explained by a thermodynamic promotion of the reactions #3, #4 and #6. However, the yield of CO also increased with the absolute pressure, despite the fact that the promotion of the reactions #2, #3, and #6 leads to a certain consumption of CO . This fact seems to confirm that the kinetics of the reaction #5 (steam gasification) can definitely be enhanced by an increase in the absolute pressure, leading to an additional formation of CO and H_2 at the expense of a certain amount of char. The higher yield of H_2 (when pressure was raised) can also be explained by a higher rate of the reaction #1 (water-

gas-shift). In line with this, Hla et al. [32] already reported an enhancement of the kinetics of the water-gas-shift reaction when pressure was increased.

From the regression coefficients listed in Table 3, it can be seen that the pyrolysis atmosphere had a statistically significant effect on the yields of both CO₂ and CO. When a pyrolysis atmosphere mainly composed of CO₂ was used, a higher yield of CO at the expense of CO₂ was observed. This finding, which was already reported in previous studies [13,14], could be explained by an enhancement of the reverse Boudouard reaction under an atmosphere of carbon dioxide. Despite the fact that the rate of the reverse Boudouard reaction is very low at temperatures below 900° C [33], the AAEMs present in the biomass feedstock as well as the nickel-rich alloy (Monel 400, from which the sample basket is made) can catalyze this reaction even at the temperatures used in the present work.

4. Conclusions

From the results presented and discussed above, the following conclusions can be drawn:

- (i) Pyrolysis peak temperature is confirmed as the most influential factor on the potential stability of biochar (i.e., carbon sequestration potential), since its effect on all the variables related to the biochar stability was statistically significant. However, the curvature term was significant for almost all these response variables, suggesting that the optimal peak temperature (at which the carbon sequestration potential is maximized) could be lower than the highest value of 600 °C. Further studies are required to establish the most appropriate peak temperature as a function of the response variable (e.g., “*stable C*”) for a given biomass feedstock.
- (ii) On the basis of the statistical outcomes reported herein, the negative effect of the absolute pressure on the yield of biochar is confirmed. In other words, keeping constant the

residence time of the gaseous phase within the pyrolysis reactor, an increase in pressure leads to a slightly decrease in the yield of biochar. Nevertheless, the most significant effect of increasing the absolute pressure was the higher production of pyrolysis gas at the expense of the produced water.

- (iii) The use of a pyrolysis atmosphere mainly composed of CO₂ instead of N₂ did not result in any remarkable change in neither the distribution of the pyrolysis products nor the potential stability of the produced biochar. However, working under an atmosphere of CO₂ resulted in a significant increase in the cumulative yield of CO at the expense of produced CO₂, leading to an interesting improvement in the composition of the produced gas.
- (iv) In summary, it seems reasonable to further explore the possibility of processing biomass through pressurized slow pyrolysis under an atmosphere of CO₂ (or the typical composition of an exhaust gas), since this process can lead to important benefits for scaling-up purposes. In this context, further research is needed in determining the optimal set of operating conditions for a given purpose (e.g., carbon sequestration potential) and for a given biomass feedstock.

Acknowledgements

The authors wish to acknowledge financial support from the Spanish MINECO-DGI (Project ENE2013-47880-C3-1-R). JJM also express his gratitude to the Aragon Government (GPT group) and the European Social Fund for additional financial support.

Appendix A. Supplementary data

Table S1: Matrix of the factorial design adopted in the present study.

Table S2: Experimental results obtained from the factorial design of experiments for the biochar yield and the response variables related to the carbon sequestration potential (x_{FC} , molar H:C ratio, molar O:C ratio, R_{50} index, and “stable C”).

Table S3: Experimental results for the yield of gas (y_{gas}), yield of produced water (y_{water}), yield of condensable organic fraction (y_{org}), and cumulative yields of the main gaseous species (CO₂, CO, CH₄ and H₂).

References

- [1] F. Verheijen, S. Jeffery, A.C. Bastos, M. van der Velde, I. Diafas, Biochar Application to Soils – A Critical Scientific Review of Effects on Soil Properties, Processes and Functions, Office for the Official Publications of the European Communities, Luxembourg, 2010.
- [2] J.J. Manyà, Pyrolysis for Biochar Purposes: A Review to Establish Current Knowledge Gaps and Research Needs, *Environ. Sci. Technol.* 46 (2012) 7939–7954.
- [3] W. Song, M. Guo, Quality variations of poultry litter biochar generated at different pyrolysis temperatures, *J. Anal. Appl. Pyrolysis* 94 (2012) 138–145.
- [4] J.J. Manyà, D. Alvira, M. Azuara, D. Bernin, N. Hedin, Effects of Pressure and the Addition of a Rejected Material from Municipal Waste Composting on the Pyrolysis of Two-Phase Olive Mill Waste, *Energy Fuels* 30 (2016) 8055–8064.
- [5] M.J. Antal, S.G. Allen, X. Dai, B. Shimizu, M.S. Tam, M. Gronli, Attainment of the Theoretical Yield of Carbon from Biomass, *Ind. Eng. Chem. Res.* 39 (2000) 4024–4031.
- [6] E.S. Noumi, J. Blin, J. Valette, P. Rousset, Combined Effect of Pyrolysis Pressure and

- Temperature on the Yield and CO₂ Gasification Reactivity of Acacia Wood in macro-TG, *Energy Fuels* 29 (2015) 7301–7308.
- [7] J. Recari, C. Berruenco, S. Abelló, D. Montané, X. Farriol, Effect of temperature and pressure on characteristics and reactivity of biomass-derived chars, *Bioresour. Technol.* 170 (2014) 204–210.
- [8] P. Rousset, C. Figueiredo, M. De Souza, W. Quirino, Pressure effect on the quality of eucalyptus wood charcoal for the steel industry: A statistical analysis approach, *Fuel Process. Technol.* 92 (2011) 1890–1897.
- [9] Y. Qian, J. Zhang, J. Wang, Pressurized pyrolysis of rice husk in an inert gas sweeping fixed-bed reactor with a focus on bio-oil deoxygenation, *Bioresour. Technol.* 174 (2014) 95–102.
- [10] J.J. Manyà, S. Laguarda, M.A. Ortigosa, J.A. Manso, Biochar from Slow Pyrolysis of Two-Phase Olive Mill Waste: Effect of Pressure and Peak Temperature on its Potential Stability, *Energy Fuels* 28 (2014) 3271–3280.
- [11] J.J. Manyà, M.A. Ortigosa, S. Laguarda, J.A. Manso, Experimental study on the effect of pyrolysis pressure, peak temperature, and particle size on the potential stability of vine shoots-derived biochar, *Fuel* 133 (2014) 163–172.
- [12] M. Azuara, B. Bager, J.I. Villacampa, N. Hedin, J.J. Manyà, Influence of pressure and temperature on key physicochemical properties of corn stover-derived biochar, *Fuel*. 186 (2016) 525–533.
- [13] G. Pilon, J.M. Lavoie, Pyrolysis of Switchgrass (*Panicum virgatum* L.) at Low Temperatures within N₂ and CO₂ Environments: Product Yield Study., *ACS Sustain. Chem. Eng.* 1 (2013) 198–204.
- [14] M. Azuara, E. Sáiz, J.A. Manso, F.J. García-Ramos, J.J. Manyà, Study on the effects of using

- a carbon dioxide atmosphere on the properties of vine shoots-derived biochar, *J. Anal. Appl. Pyrolysis* 124 (2017) 719–725.
- [15] O.R. Harvey, L.J. Kuo, A.R. Zimmerman, P. Louchouart, J.E. Amonette, B.E. Herbert, An Index-Based Approach to Assessing Recalcitrance and Soil Carbon Sequestration Potential of Engineered Black Carbons (Biochars), *Environ. Sci. Technol.* 46 (2012) 1415–1421.
- [16] K. Crombie, O. Masek, S.P. Sohi, P. Brownsort, A. Cross, The effect of pyrolysis conditions on biochar stability as determined by three methods, *GCB Bioenergy* 5 (2013) 122–131.
- [17] A. Cross, S.P. Sohi, A method for screening the relative long-term stability of biochar, *GCB Bioenergy* 5 (2013) 215–220.
- [18] M. Rhodes, *Introduction to Particle Technology: Second Edition*, John Wiley & Sons, Ltd, Chichester, UK, 2008.
- [19] L. Wang, O. Skreiberg, M. Gronli, G.P. Specht, M.J. Antal, Is Elevated Pressure Required to Achieve a High Fixed-Carbon Yield of Charcoal from Biomass? Part 2: The Importance of Particle Size, *Energy Fuels* 27 (2013) 2146–2156.
- [20] G.B. García, M. Calero De Hoces, C. Martínez García, M.T. Cotes Palomino, A.R. Gálvez, M.Á. Martín-Lara, Characterization and modeling of pyrolysis of the two-phase olive mill solid waste, *Fuel Process. Technol.* 126 (2014) 104–111.
- [21] I. Mediavilla, M.J. Fernández, L.S. Esteban, Optimization of pelletisation and combustion in a boiler of 17.5 kWth for vine shoots and industrial cork residue, *Fuel Process. Technol.* 90 (2009) 621–628.
- [22] S. Mani, L.G. Tabil, S. Sokhansanj, Grinding performance and physical properties of wheat and barley straws, corn stover and switchgrass, *Biomass Bioenergy* 27 (2004) 339–352.
- [23] D.C. Montgomery, *Design and analysis of experiments: 6th ed.*, John Wiley & Sons,

Hoboken, NJ, 2005.

- [24] C. Di Blasi, G. Signorelli, C. Di Russo, G. Rea, Product Distribution from Pyrolysis of Wood and Agricultural Residues, *Ind. Eng. Chem. Res.* 38 (1999) 2216–2224.
- [25] O. Mašek, P. Brownsort, A. Cross, S. Sohi, Influence of production conditions on the yield and environmental stability of biochar, *Fuel* 103 (2013) 151–155.
- [26] F. Ronsse, S. van Hecke, D. Dickinson, W. Prins, Production and characterization of slow pyrolysis biochar: influence of feedstock type and pyrolysis conditions, *GCB Bioenergy* 5 (2013) 104–115..
- [27] Y. Wang, Y. Hu, X. Zhao, S. Wang, G. Xing, Comparisons of Biochar Properties from Wood Material and Crop Residues at Different Temperatures and Residence Times, *Energy Fuels* 27 (2013) 5890–5899.
- [28] L. Zhao, X. Cao, O. Mašek, A. Zimmerman, Heterogeneity of biochar properties as a function of feedstock sources and production temperatures, *J. Hazard. Mater.* 256–257 (2013) 1–9.
- [29] F.-X. Collard, J. Blin, A review on pyrolysis of biomass constituents: Mechanisms and composition of the products obtained from the conversion of cellulose, hemicelluloses and lignin, *Renew. Sustain. Energy Rev.* 38 (2014) 594–608.
- [30] R. Ragucci, P. Giudicianni, A. Cavaliere, Cellulose slow pyrolysis products in a pressurized steam flow reactor, *Fuel* 107 (2013) 122–130.
- [31] K. Matsuoka, D. Kajiwara, K. Kuramoto, A. Sharma, Y. Suzuki, Factors affecting steam gasification rate of low rank coal char in a pressurized fluidized bed, *Fuel Process. Technol.* 90 (2009) 895–900.
- [32] S.S. Hla, G.J. Duffy, L.D. Morpeth, A. Cousins, D.G. Roberts, J.H. Edwards, Investigation of the effect of total pressure on performance of the catalytic water–gas shift reaction using

simulated coal-derived syngases, *Catal. Commun.* 11 (2009) 272–275.

- [33] P. Lahijani, Z.A. Zainal, M. Mohammadi, A.R. Mohamed, Conversion of the greenhouse gas CO₂ to the fuel gas CO via the Boudouard reaction: A review, *Renew. Sustain. Energy Rev.* 41 (2015) 615–632.

Table 1

Proximate, elemental and XRF analyses of the biomass sources (CS, TPOMW, and VS).

Proximate	CS	TPOMW	VS
Moisture (wt. %)	7.27 ± 0.31	12.8 ± 0.12	7.97 ± 0.68
Ash (wt. % in dry basis)	2.70 ± 0.20	2.27 ± 0.11	1.08 ± 0.05
Volatile matter (wt. % in dry basis)	86.6 ± 0.11	87.5 ± 1.95	74.0 ± 1.19
Fixed carbon (wt. % in dry basis)	10.7 ± 0.49	10.2 ± 1.13	24.9 ± 1.91
Elemental (wt. % in daf ^a basis) ^b	CS	TPOMW	VS
C	44.4 ± 0.31	50.0 ± 0.48	47.1 ± 0.14
H	5.60 ± 0.04	6.21 ± 0.17	5.29 ± 0.09
N	0.43 ± 0.01	2.29 ± 0.09	0.66 ± 0.05
S	0.45 ± 0.05	0.40 ± 0.07	0.56 ± 0.13
Inorganic matter (wt.% of ash)	CS	TPOMW	VS
CaO	30.7 ± 0.23	43.3 ± 0.25	58.3 ± 0.25
K ₂ O	9.85 ± 0.15	33.7 ± 0.24	18.4 ± 0.12
MgO	3.45 ± 0.17	1.65 ± 0.14	6.66 ± 0.14
SiO ₂	31.4 ± 0.23	4.34 ± 0.10	5.73 ± 0.08
Fe ₂ O ₃	6.49 ± 0.12	2.91 ± 0.08	3.51 ± 0.11
Al ₂ O ₃	4.85 ± 0.12	1.60 ± 0.07	2.57 ± 0.07
P ₂ O ₅	4.13 ± 0.10	4.33 ± 0.10	1.24 ± 0.04
PbO	2.50 ± 0.08	0.55 ± 0.06	0.26 ± 0.02
S (inorganic)	1.94 ± 0.07	4.26 ± 0.01	0.60 ± 0.03
Cl (inorganic)	0.59 ± 0.03	0.37 ± 0.02	0.48 ± 0.02
MnO	0.53 ± 0.03	0.31 ± 0.03	0.53 ± 0.03
ZnO	0.24 ± 0.02	0.14 ± 0.02	0.32 ± 0.02
SnO ₂	0.45 ± 0.03	0.33 ± 0.03	0.26 ± 0.02
TiO ₂	0.59 ± 0.03	0.20 ± 0.02	0.34 ± 0.02
CuO	0.08 ± 0.02	0.26 ± 0.03	0.09 ± 0.01
MoO ₃	0.28 ± 0.02	0.25 ± 0.02	0.02 ± 0.01
La ₂ O ₃	0.23 ± 0.04	0.31 ± 0.04	ND ^c
Y ₂ O ₃	0.26 ± 0.02	ND	ND

^a Dry-ash-free.^b Oxygen is calculated by difference.^c Not detected.

Table 2

Summary statistics for the regression models based on the data given in Table S2 (values in brackets correspond to the p -values resulting from t -tests; significant terms are marked in bold).

Coefficient	Response variable					
	y_{char}^d	x_{FC}^e	$H:C$ ratio	$O:C$ ratio	R_{50} index	Stable C
β_0	0.350	0.813	0.437	0.104	0.542	79.6
<i>Block 1 (CS)</i>	-0.015 (0.000)	0.026 (0.001)	-0.039 (0.000)	0.009 (0.176)	0.007 (0.165)	6.09 (0.000)
<i>Block 2 (VS)</i>	-0.007 (0.034)	-0.024 (0.002)	0.030 (0.000)	0.001 (0.935)	-0.015 (0.004)	-6.93 (0.000)
<i>Block 3 (TPOMW)</i>	0.022 (0.000)	-0.002 (0.739)	0.009 (0.172)	-0.010 (0.153)	0.008 (0.093)	0.842 (0.373)
β_1 (T)	-0.030 (0.000)	0.055 (0.000)	-0.141 (0.000)	-0.043 (0.000)	0.027 (0.000)	6.52 (0.000)
β_2 (P)	-0.009 (0.001)	0.022 (0.001)	-0.014 (0.016)	-0.010 (0.092)	0.006 (0.168)	-0.375 (0.630)
β_3 (CO ₂)	-0.001 (0.580)	0.004 (0.487)	-0.038 (0.002)	-0.005 (0.409)	0.003 (0.493)	0.325 (0.676)
β_{12} (T·P)	-0.002 (0.514)	0.011 (0.069)	-0.004 (0.472)	0.000 (0.940)	-0.001 (0.813)	-0.292 (0.708)
β_{13} (T·CO ₂)	-0.002 (0.535)	-0.002 (0.719)	0.001 (0.806)	0.001 (0.916)	0.002 (0.630)	0.025 (0.974)
β_{23} (P·CO ₂)	0.001 (0.801)	0.000 (0.971)	0.002 (0.650)	0.002 (0.717)	0.001 (0.781)	0.083 (0.915)
β_{123} (T·P·CO ₂)	0.002 (0.472)	-0.001 (0.854)	0.001 (0.852)	-0.001 (0.856)	0.000 (0.943)	0.067 (0.932)
<i>Overall Curvature</i>	-0.017 (0.001)	0.025 (0.027)	-0.041 (0.001)	-0.042 (0.001)	-0.003 (0.695)	3.23 (0.039)
<i>Adj. R²</i>	0.874	0.805	0.957	0.703	0.604	0.808

^d Mass fraction in daf basis.

^e Mass fraction.

Table 3

Summary statistics for the regression models based on the data given in Table S3 (values in brackets correspond to the p -values resulting from t -tests; significant terms are marked in bold).

Coefficient	Response variable						
	y_{gas}^f	y_{water}^f	y_{org}^f	$y_{CO_2}^g$	y_{CO}^g	$y_{CH_4}^g$	$y_{H_2}^g$
β_0	0.308	0.156	0.191	3.731	2.655	1.397	0.722
<i>Block 1 (CS)</i>	0.006 (0.425)	0.004 (0.566)	0.005 (0.519)	-0.035 (0.580)	0.315 (0.006)	0.070 (0.148)	0.094 (0.168)
<i>Block 2 (VS)</i>	-0.041 (0.000)	0.042 (0.000)	0.001 (0.910)	-0.457 (0.000)	-0.405 (0.001)	-0.118 (0.020)	-0.108 (0.117)
<i>Block 3 (TPOMW)</i>	0.036 (0.000)	-0.045 (0.000)	-0.006 (0.450)	0.492 (0.000)	0.090 (0.397)	0.048 (0.321)	0.014 (0.839)
$\beta_1 (T)$	0.035 (0.000)	0.002 (0.717)	-0.006 (0.386)	0.305 (0.000)	0.333 (0.001)	0.253 (0.000)	0.389 (0.000)
$\beta_2 (P)$	0.036 (0.000)	-0.028 (0.000)	-0.002 (0.795)	0.372 (0.000)	0.420 (0.000)	0.261 (0.000)	0.244 (0.000)
$\beta_3 (CO_2)$	0.006 (0.326)	0.004 (0.534)	-0.001 (0.852)	-0.154 (0.007)	0.315 (0.001)	-0.040 (0.320)	-0.051 (0.366)
$\beta_{12} (T \cdot P)$	-0.005 (0.405)	0.000 (0.994)	0.000 (0.995)	-0.036 (0.492)	0.011 (0.897)	-0.036 (0.361)	0.026 (0.643)
$\beta_{13} (T \cdot CO_2)$	0.002 (0.724)	0.001 (0.859)	0.004 (0.592)	-0.080 (0.135)	0.044 (0.617)	0.026 (0.507)	-0.059 (0.294)
$\beta_{23} (P \cdot CO_2)$	0.000 (0.972)	0.000 (0.920)	-0.003 (0.660)	0.007 (0.893)	0.161 (0.075)	-0.072 (0.077)	0.014 (0.799)
$\beta_{123} (T \cdot P \cdot CO_2)$	0.001 (0.884)	-0.004 (0.413)	-0.003 (0.643)	0.042 (0.426)	0.030 (0.727)	0.017 (0.665)	-0.006 (0.917)
<i>Overall Curvature</i>	0.009 (0.453)	-0.001 (0.939)	0.005 (0.722)	0.184 (0.077)	0.171 (0.310)	-0.037 (0.623)	0.247 (0.028)
<i>Adj. R²</i>	0.765	0.717	0.000	0.841	0.666	0.738	0.688

^f Mass fraction in daf basis.

^g In mmol g⁻¹ daf feedstock.

Table 4

Main reactions involved during the release of the pyrolysis gas.

No.	Reaction	Extent of reaction (kmol) ^h	
		600 °C and 0.1 MPa	600 °C and 1.0 MPa
1	$H_2O + CO \rightleftharpoons CO_2 + H_2$	0.244	0.244
2	$2CO \rightleftharpoons CO_2 + C$	0.715	0.908
3	$3H_2 + CO \rightleftharpoons CH_4 + H_2O$	0.063	0.669
4	$C + 2H_2 \rightleftharpoons CH_4$	-0.212	0.532
5	$C + H_2O \rightleftharpoons CO + H_2$	-0.136	-0.700
6	$2H_2 + 2CO \rightleftharpoons CO_2 + CH_4$	0.148	0.705

^h Calculated using Aspen Plus V8.8; NRTL package and a Gibbs Reactor module. Stoichiometric coefficients were taken as initial molar flow rates (in kmol h⁻¹) for all the species involved in the reaction.

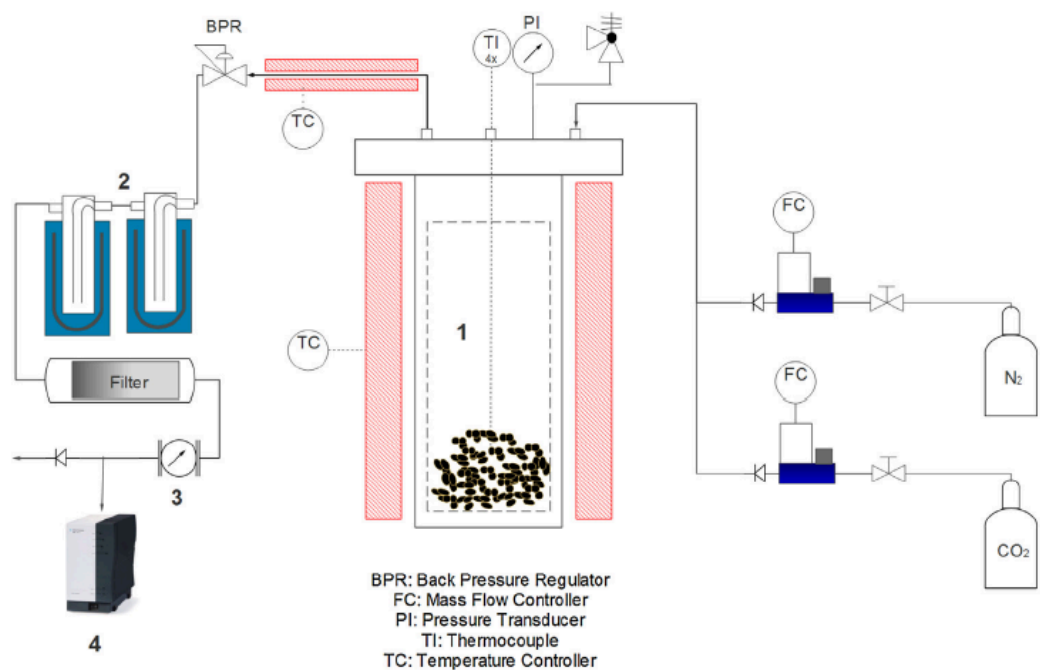


Fig. 1. Schematic of the pressurized pyrolysis device: (1) fixed-bed pyrolysis reactor, (2) pyrolysis liquid condensation system, (3) volumetric gas meter, and (4) micro-GC.

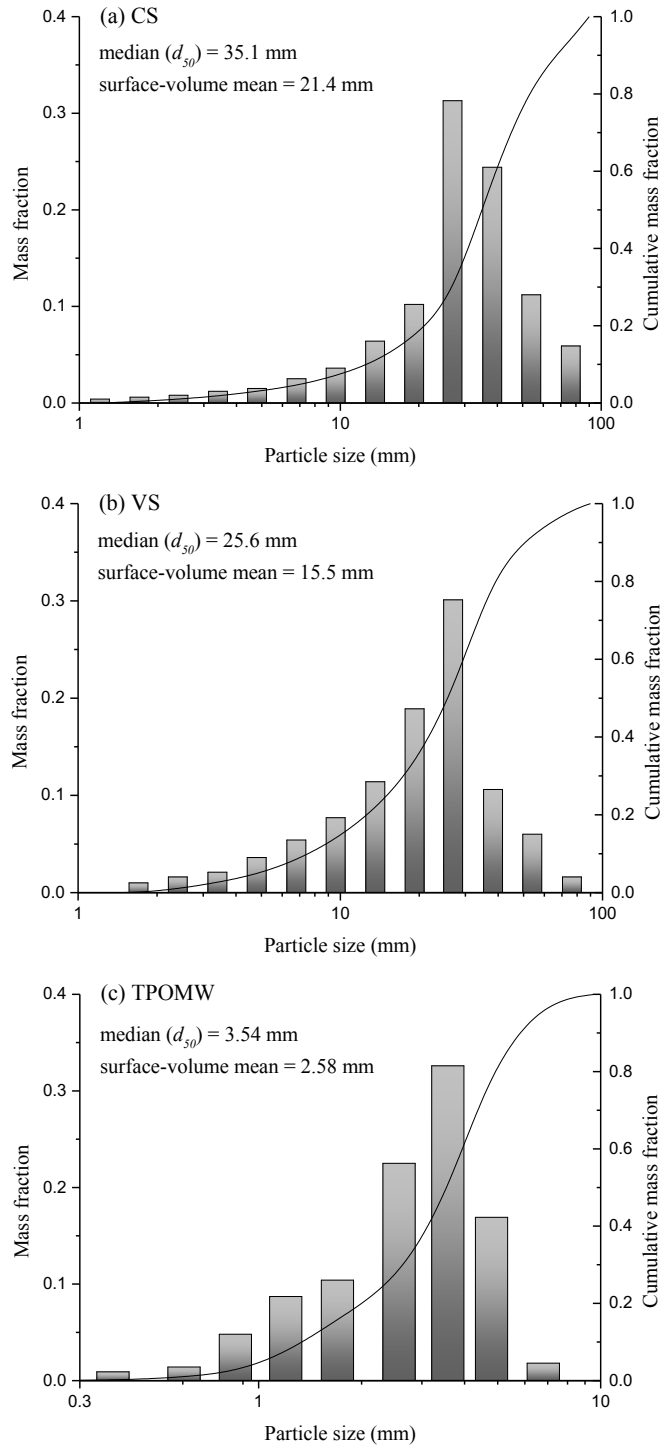


Fig. 2. Particle size distributions of the biomass sources used in the present study: (a) CS, (b) VS, and (c) TPOMW. The d_{50} (median) and surface-volume mean (harmonic mean [18]) values are shown in the corresponding plot.

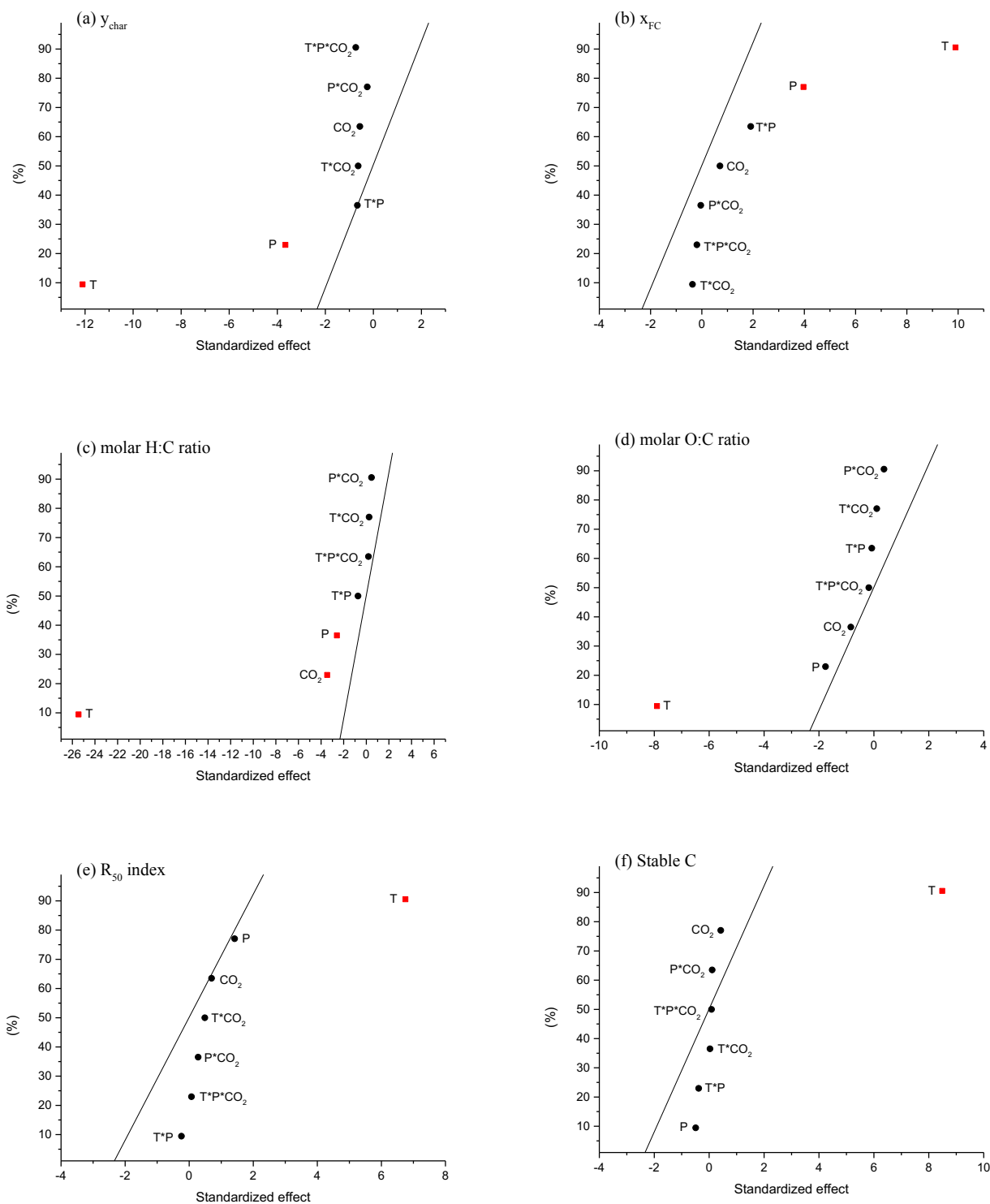


Fig. 3. Normal plots of standardized effects ($\alpha = 0.05$) for (a) y_{char} , (b) x_{FC} , (c) molar H:C ratio, (d) molar O:C ratio, (e) R_{50} index, and (f) “stable C”.

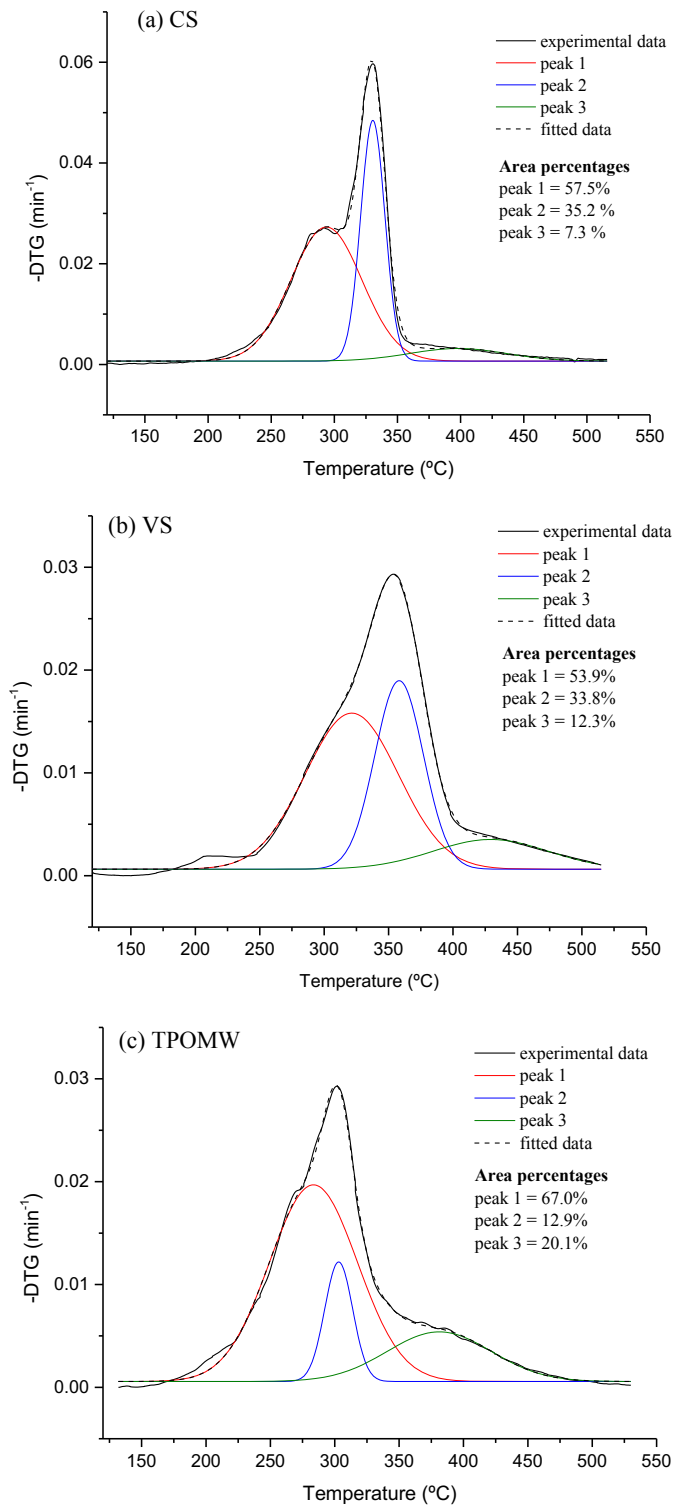


Fig 4. Deconvoluted DTG curves for the pyrolysis of (a) corn stover (CS), (b) vine shoots (VS), and (c) two-phase olive mill waste (TPOMW).

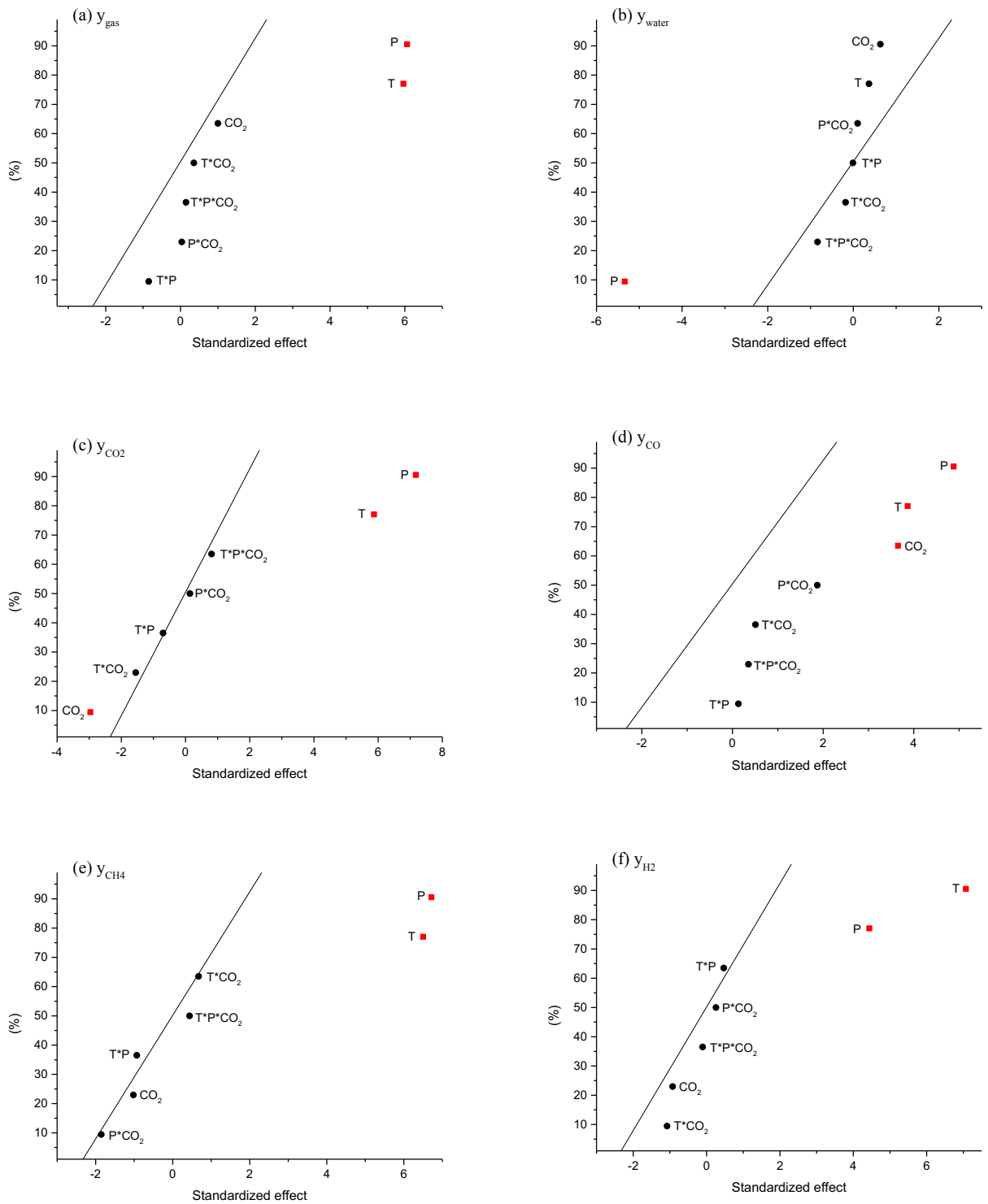


Fig. 5. Normal plots of standardized effects ($\alpha = 0.05$) for (a) y_{gas} , (b) y_{water} , (c) y_{CO_2} , (d) y_{CO} , (e), y_{CH_4} , and (f) y_{H_2} .